Understanding co-effects of manganese and cobalt on the enhanced SCR performance for $Mn_xCo_{1-x}Cr_2O_4$ spinel-type catalysts

Erhao Gao[a,b], Bei Huang[a,b], Zilong Zhao[c], Hua Pan[c], Wei Zhang[a,b], Younan Li[a,b], Matthew T. Bernards[d], Yi He[a,e], and Yao Shi[a,b]*

[a] College of Chemical and Biological Engineering, Zhejiang University, Hangzhou, 310027, China

[b] Key Laboratory of Biomass Chemical Engineering of Ministry of Education, Zhejiang University, Hangzhou, China

[c] College of Biology and Environmental Engineering, Zhejiang Shuren University, Hangzhou 310015, China

[d] Department of Chemical and Materials Engineering, University of Idaho, Moscow 83844, USA

[e] Department of Chemical Engineering, University of Washington, Seattle, Washington 98195, USA

Characterization and theoretical computation

Catalyst Characterization

X-ray diffraction (XRD) patterns were characterized by an Ultima IV XRD powder polycrystalline diffractometer with a scanning rate of 1°C min^{-1}. Raman spectra were obtained with a Jobin-Yvon LabRamHRUV spectrometer with a scanning range of 100-800 cm^{-1}. N_2 adsorption-desorption isotherms were obtained at 77 K with a Micromeritics ASAP-2460. The samples were treated with pure nitrogen at 400 °C for 1 h before the analysis. X-ray photoelectron spectroscopy (XPS) data were obtained with a Thermo ESCALAB 250XI electron spectrometer. The binding energies were referenced to the C 1s line at 284.8 eV from adventitious carbon. Scanning electron microscopy (SEM) micrographs of the samples were recorded with a Zeiss SIGMA HD, and the elemental distribution of the samples were characterized with energy-dispersive X-ray (EDX) analysis. The data for ammonia temperature-programmed desorption (NH_3-TPD), and hydrogen temperature-programmed reduction (H_2-TPR) were recorded on an AutoChem II 2920 with a thermal conductivity detector (TCD). The samples were pretreated at 400 °C in He for 1 h prior to the experiments. For the NH_3-TPD experiments, the samples were exposed to a flow of 10% vol. NH_3 in He for 1 h, then NH_3 residues in the reactor were removed by a pure He purge for 0.5 h. Finally, the temperature was raised from 30 to 450°C in He at a rate of 10°C min^{-1}. For H_2-TPR experiments, the samples were also cooled down to room temperature, then the temperature was raised from 30 to 800°C at a rate of 10°C min^{-1} in a flow of 5 vol.% H_2 in He.

Theoretical computation

All calculations were performed based on DMol[3] implemented in Materials Studio 2017[R2] [1], in which the Perdew-Burke-Ernzerhoff (PBE) [2] functional in generalized gradient approximation (GGA) [3] was used to calculate the exchange-correlation potential. The following three convergence criteria were used for the geometry optimization and energy calculation: the atomic forces (2.0×10^{-3} Hartree/Å), maximum displacement (5.0×10^{-3} Å), and total energy variation (1.0×10^{-5} Hartree). The molecular orbitals were expanded using a double numerical basis set with polarization functions (DNP). The core electrons were treated using the DFT semi-core pseudopots (DSPP) method. The Monkhorst-Pack k-point grid was set as a 3 × 3 × 1. A p(2 × 2) slab exposing the (100) plane of $CoCr_2O_4$ with six atomic layers in this work. A 15 Å vacuum layer was placed above the surface slab to avoid interference from the imaging surface slabs [4]. The bottom three layers were fixed while the top three layers were relaxed during the calculation. The affinity between the surface and adsorbate is reflected by adsorption energy (E_{ads}), which is defined as:

$$E_{ads} = E_{sub} + E_x - E_{total}$$

Where E_{sub} and E_x denote the energy of catalyst model and gas molecule, respectively, and E_{total} denotes the total energy of the system. A smaller value of E_{ads} indicates a stronger adsorption affinity.

XPS analysis

The Co $2p_{3/2}$ XPS spectra were fit with three peaks. The sub-band at 780.4-780.7 eV was assigned to Co^{3+}, the sub-band at 782.4-783.0 eV was assigned to Co^{2+}, and the sub-band around 786.8 eV was the satellite peak of Co^{2+} [5]. The Mn $2p_{3/2}$ were fit with three peaks representing Mn^{2+} (640.0-640.5 eV), Mn^{3+} (641.2-641.8 eV), and Mn^{4+} (642.5-643.3 eV), respectively [6-8]. The Cr $2p_{3/2}$ spectra were fit with three peaks. The bands centered at 575.5-575.7 eV, 576.7-576.9 eV, and 578.9-579.2 eV were attributed to Cr^{2+}, Cr^{3+}, and Cr^{5+}, respectively [9-11]. The O 2p spectra were fit with two peaks representing chemisorbed oxygen (531.4-531.6 eV, denoted as O_{α}) and lattice oxygen species (530.3-530.5 eV, denoted as O_{β}) [12].

Table S1. A comparison of T_{90} operating windows over various SCR catalysts and different GHSVs

Catalyst samples	**T_{90} operation window**	**GHSV**	**Ref.**
$Mn_{0.1}Co_{0.9}Cr_2O_4$	166-393 °C	112,000 h^{-1}	This work
	199-384 °C	162,000 h^{-1}	
V_2O_5-WO_3/TiO_2	260-425 °C	60,000 h^{-1}	Appl. Catal. B-Environ. 168-169 (2015): 195-202
Mn-Ni bi-metal oxide	125-275 °C	64,000 h^{-1}	Appl. Catal. B-Environ. 148-149 (2014) 114-122.
$Mn_{0.05}Co_{0.95}O_x$	160-190 °C	60,000 h^{-1}	J. Phys. Chem. C. 119 (2015) 22924-22933.
$Mn_xCo_{3-x}O_4$ nanocages	125-350 °C	38,000 h^{-1}	ACS Catal. 4 (2014) 1753-1763.
3D-$MnCo_2O_4$	90-250 °C	32,000 h^{-1}	Nanoscale 7 (2015) 2568-2577.
Mn_2CoO_4@rGO	130-200 °C	30,000 h^{-1}	Chem. Eng. J. 333 (2018) 467-476.
Sphere-like $Mn_xCo_{3-x}O_4$	200-300 °C	23,000 h^{-1}	Ind. Eng. Chem. Res. 50 (2011) 6668–6672.
Co_3O_4 nanorods	135-215 °C	30,000 h^{-1}	Appl. Catal. B-Environ. 129 (2013) 491-500.
Co(3)-Mn/TiO_2	200-275 °C	40,000 h^{-1}	ACS Catal. 5 (2015) 6069−6077.
$Ce_{0.8}W_{0.2}O_x$	215-420 °C	125,000 h^{-1}	J. Mater. Chem. A. 8 (2020) 6717-6731

Table S2. Calculated bond length (d; Å), Mulliken charge (q; e), and adsorption energy (E_{ads}; eV) for NH_3 adsorption on $CoCr_2O_4$ and $Mn_{0.1}Co_{0.9}Cr_2O_4$ catalysts.

	NH_3-$CoCr_2O_4$			NH_3-$Mn_{0.1}Co_{0.9}Cr_2O_4$			
	Co site	Cr site	OH site	Co site	Cr site	Mn site	OH site
$d_{N\text{-}Metal}/d_{O\text{-}H}$	2.062	2.150	1.278	2.054	2.140	2.201	1.045
$d_{N\text{-}H1}$	1.025	1.023	1.022	1.023	1.023	1.023	1.022
$d_{N\text{-}H2}$	1.022	1.023	1.023	1.017	1.024	1.023	1.022
$d_{N\text{-}H3}$	1.030	1.023	1.022	1.038	1.023	1.031	1.034
q_{NH3}	0.268	0.280	0.285	0.272	0.297	0.314	0.291
E_{ads}	-0.87	-0.75	-0.98	-0.97	-0.95	-1.36	-1.19

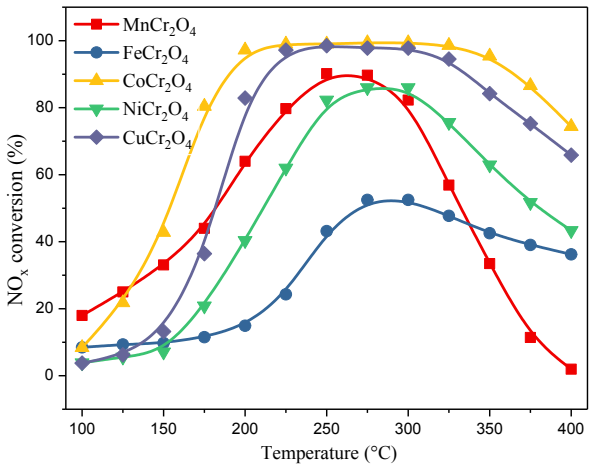

Figure S1. NO_x conversion over XCr_2O_4 (X = Mn, Fe, Co, Ni, and Cu) catalysts in the temperature range of 100 to 400 °C.

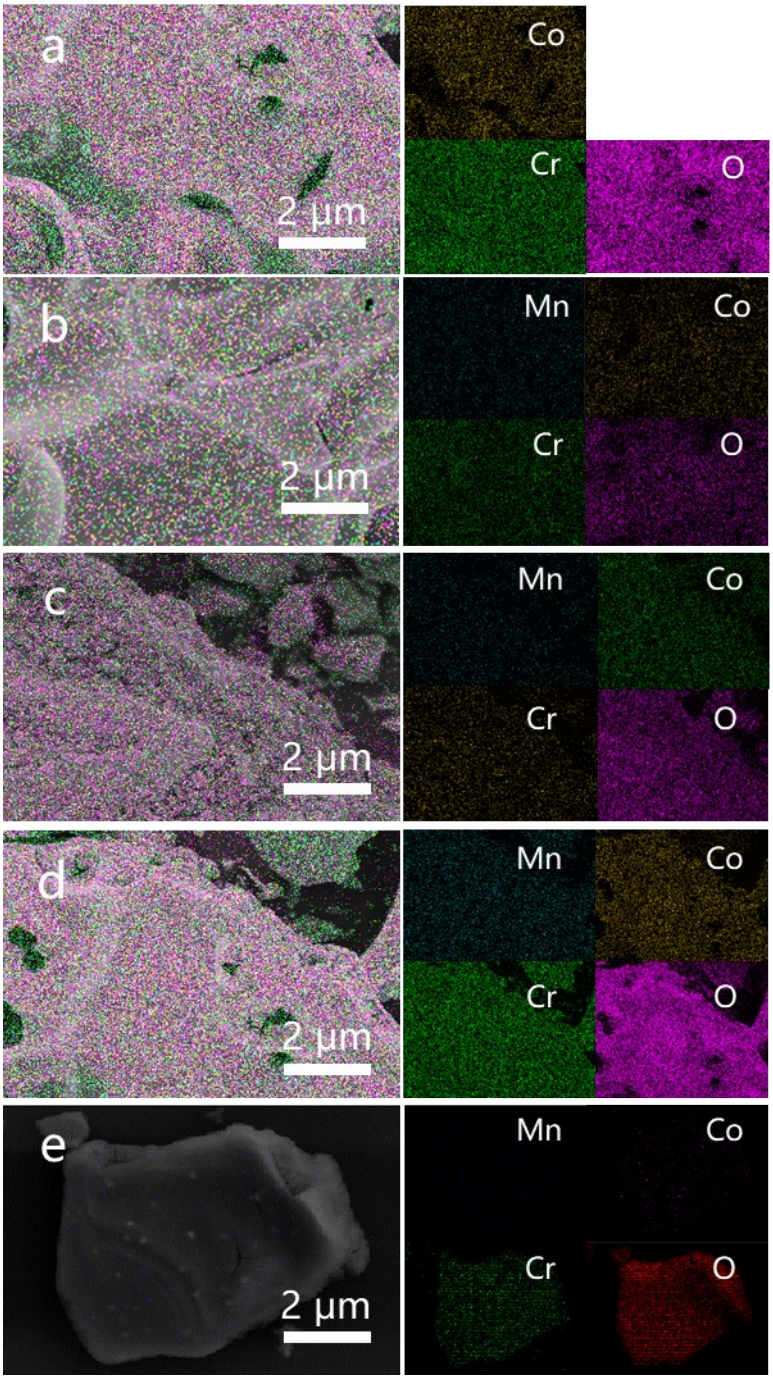

Figure S2. Representative energy-dispersive X-ray (EDX) spectroscopy elemental mapping of different elemental species distribution in (a) $CoCr_2O_4$, (b) $Mn_{0.05}Co_{0.95}Cr_2O_4$, (c) $Mn_{0.1}Co_{0.9}Cr_2O_4$, (d) $Mn_{0.2}Co_{0.8}Cr_2O_4$, and (e) $Mn_{0.3}Co_{0.7}Cr_2O_4$ catalysts.

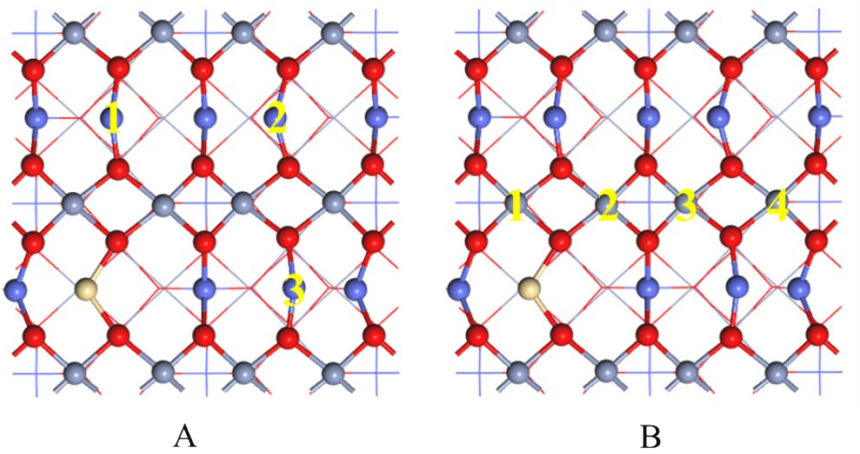

Figure S3. All of the possible adsorption sites for (A) Co and (B) Cr cations in the $Mn_{0.1}Co_{0.9}Cr_2O_4$ model.

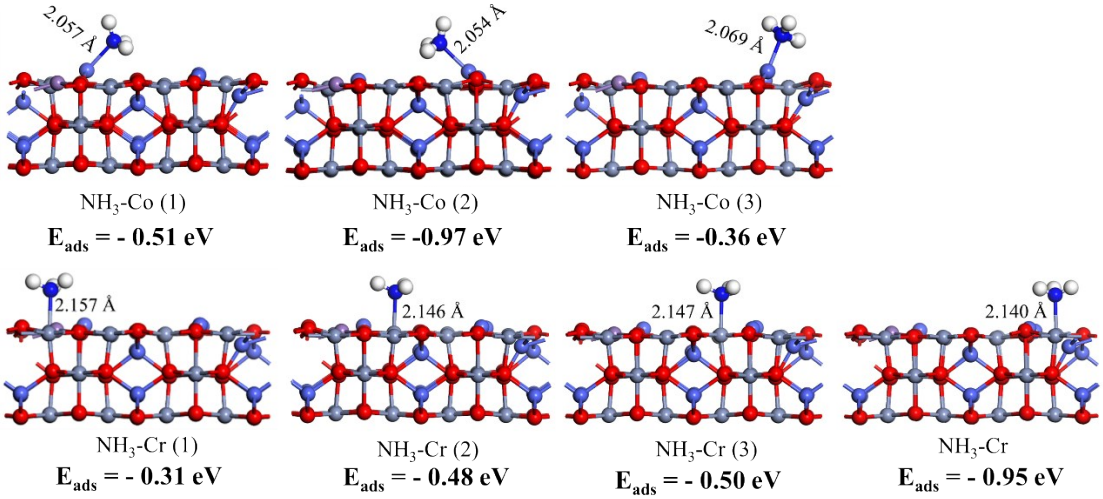

Figure S4. The optimized structures of adsorbed NH_3 on all of the possible Co and Cr sites on $Mn_{0.1}Co_{0.9}Cr_2O_4$ model

The effect of internal diffusion on $Mn_{0.1}Co_{0.9}Cr_2O_4$ catalyst was studied and the results are presented in Figure S5. The catalysts with particle sizes of 80-100, 60-80, 40-60, and 20-40 meshes were prepared respectively and tested at 200 °C. It can be seen that when the particle size was 80-100 meshes, 60-80 meshes and 40-60 meshes, the NO_x conversion was around 99%, while the NO_x conversion decreased to 90.5% when the particle sizes were 20-40 meshes. The particle sizes of $Mn_{0.1}Co_{0.9}Cr_2O_4$ catalyst tested were 40-60 meshes in this work, which suggests that the internal diffusion was eliminated under this condition.

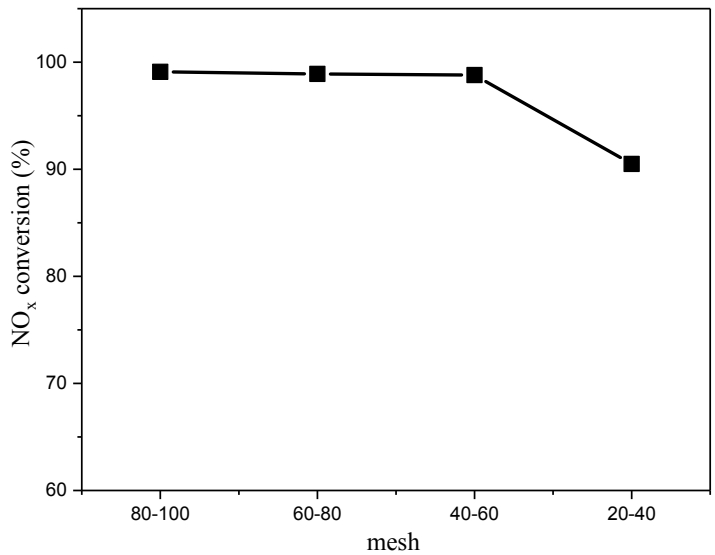

Figure S5. The effect of internal diffusion on $Mn_{0.1}Co_{0.9}Cr_2O_4$ catalyst at 200 °C

The effect of external diffusion on $Mn_{0.1}Co_{0.9}Cr_2O_4$ catalyst was studied and the results are presented in Figure S6. Samples weighing 0.1 g (W_1) and 0.15 g (W_2) were tested respectively under different GHSVs (60,000-30,000 h^{-1}). It can be seen that all the points can be connected into one curve, which suggests that the external diffusion was eliminated under the GHSV of 112,000 h^{-1}.

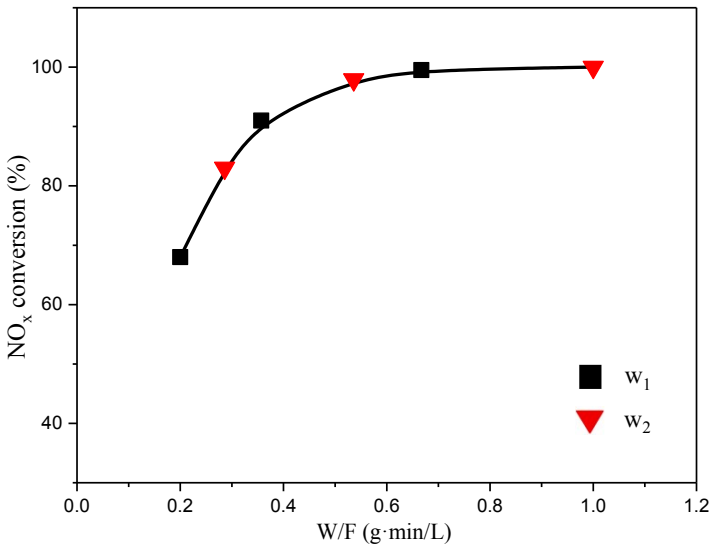

Figure S6. The effect of external diffusion on $Mn_{0.1}Co_{0.9}Cr_2O_4$ catalyst at 200 °C

References:

1. Delley, B., *The Journal of Chemical Physics*, 2000, **113**, 7756-7764.
2. Hammer, B., *Phys. Rev. B.*, 1999, **59**, 7413-7421.
3. Perdew, J.P., Burke, K. and Wang, Y., *Phys. Rev. B.*, 1996, **54**, 16533-16539.
4. Yang, Y., Liu, J., Liu, F., Wang, Z., Ding, J. and Huang, H., *Chem Eng J*, 2019, **361**, 578-587.
5. Li, X., Ao, Z., Liu, J., Sun, H., Rykov, A.I. and Wang, J., *Acs Nano*, 2016, **10**, 11532-11540.
6. Thirupathi, B. and Smirniotis, P., *Appl. Catal. B*, 2011, **110**, 195-206.
7. Wan, Y., Zhao, W., Tang, Y., Li, L., Wang, H., Cui, Y., Gu, J., Li, Y. and Shi, J., *Applied Catalysis B: Environmental*, 2014, **148-149**, 114-122.
8. Yang, S., Wang, C., Li, J., Yan, N., Ma, L. and Chang, H., *Appl Catal B-Environ*, 2011, **110**, 71-80.
9. Chen, Z., Yang, Q., Li, H., Li, X., Wang, L. and Chi Tsang, S., *J Catal*, 2010, **276**, 56-65.
10. Russo, N., Fino, D., Guido, S. and Specchia, V., *J Catal*, 2005, **229**, 459-469.
11. Biesinger, M., Payne, B., Grosvenor, A., Lau, L., Gerson, A. and Smart, R., *Appl Surf Sci*, 2011, **257**, 2717-2730.
12. Zhang, L., Shi, L., Huang, L., Zhang, J., Gao, R. and Zhang, D., *Acs Catal*, 2014, **4**, 1753-1763.